# Design and first results of a retractable 1D-CFC Beam Target for BATMAN Upgrade

G. Orozco[a], F. Bonomo[a], N. den Harder[a], B. Heinemann[a], A. Hurlbatt[a], R. Nocentini[a], R. Riedl[a], C. Wimmer[a]

[a]*Max Planck Institute for Plasma Physics, Boltzmannstrasse 2, 85748 Garching, Germany*

BATMAN Upgrade (BUG) is a test facility for the production of negative ion beams from an RF driven plasma ion source devoted to supporting the development of the ITER Neutral Beam Injection (NBI). BUG consists of the IPP RF prototype source and a multi-aperture grid system corresponding roughly to a beamlet group of the ITER NBI grid system, i.e. an arrangement of 14 (vertical) ×5 (horizontal) Ø14 mm apertures, meaning the ion beam is comprised of 70 individual beamlets. The beams can be extracted with up to 10 kV and accelerated up to a total voltage of 45 kV for up to 10 s (steady state operation is underway). One of the goals of BUG is a detailed study of the ion beam optics. So far, the permanently installed beam diagnostic consisted of several lines of sight of Beam Emission Spectroscopy (BES) at two different positions and thermocouple measurements on the beam dump calorimeter. Resolving the divergence and deflection of single beamlets is technically exceptionally difficult with the existing diagnostic tools, therefore, a beam target made out of a one-directional carbon fiber composite material (1D-CFC) with dimensions 376×142×20 mm³ has been installed at a distance of 851 mm from the exit of the grid system. The thermal footprints of the beamlets are observed from the back side via infrared imaging with a high spatial resolution (<0.7 mm/pixel) that allows characterization of the beamlets at low divergence. The target can be rotated out of the beam to make it compatible with long pulses and the forthcoming steady state operation. The safety analysis of the target operation for different operational scenarios is presented together with an energy-based interlock. Finally, the accuracy of estimating the shape of the heat flux on the front of the target from the temperature profile at the back is assessed, based on FEM simulations of a single beamlet.

Keywords: Ion beam optics, 1D-CFC, Thermography, Calorimetry, BATMAN-Upgrade.

## 1. Introduction

Each of the two Neutral Beam Injectors (NBI) to be installed in the ITER test facility will deliver 16.5 MW heating power into the torus as a superposition of a total of 1280 $H^0$ or $D^0$ beamlets, arranged in 16 beamlet groups (4 × 4) with a sub arrangement of 5(h) × 16(v). A multi-grid, multi-aperture ion beam acceleration system of up to a total of 1 MeV accelerates a total current of negative ions of 46 A for H and 40 A for D, extracted from an RF-driven plasma ion source (for a detailed description see [1]). BATMAN Upgrade (BUG) is the evolution of the prototype ion source, baseline design of that of the ITER NBI. Its beam acceleration system is equipped with a grid electrode system, mimicking back that of the ITER NBI in a size corresponding to a beamlet group arrangement with 5(h) × 14(v) beamlets but with a limited available acceleration voltage of maximum 45 kV (further details in [2]).

The accelerated beam must fulfill the requirements of high beam homogeneity and a beamlet core divergence lower than 7 mrad. The measurement of an individual beamlet divergence within a beam is difficult, therefore the current configuration of the acceleration system in BUG has 34 masked apertures out of 70, to isolate a single beamlet on the top most part of the beamlet group (see Figure 1).

One of the focus of the investigations in BUG is the beam optics. The most extensively exploited beam diagnostic tool in BUG is the noninvasive spectroscopic analysis of the light emitted by interaction of beam particles with the residual neutral gas ($H_2$ or $D_2$), called Doppler-Shift $H_\alpha$ Beam Emission Spectroscopy (BES). It delivers a line-integrated insight of the beam properties that can be complemented with more spatially resolved diagnostics, commonly more invasive like the diagnostic calorimeter that also serves as beam dump (see Figure 1).

Another common calorimetric diagnostic tool with higher spatial resolution is a target made out of a carbon composite material monitored with an IR camera. The material consists of a stacked arrangement of carbon fibers oriented in the same direction (in the target thickness), within a carbon matrix, therefore referred as 1D-CFC. The heat conduction along the fibers is up to 20 times higher than perpendicular to them. This strong heat conduction anisotropy results in sharp temperature profiles via IR imaging obtained as in BUG, from the rear side of the target which is a close representation of the heat flux of the beam on the front.

There have been experiments in the past [3] with such a beam target in the earlier version of BUG, BATMAN, within collaboration campaigns together with Consorzio RFX (Padua) in the preparation for their own beam target diagnostic (STRIKE [4]) installed in the full size test facility of ITER NBI ion source, SPIDER [5]. It was possible to compare quantitatively both BES and 1D-CFC thermography for a single beamlet, finding good agreement [6]. The configuration of the target was, however, fixed in position, 1340 mm from the beam acceleration system and partially blocking the diagnostic calorimeter, thus limiting the beam pulse length and repetition, limiting the operation of the teststand.

*author's email: guillermo.orozco@ipp.mpg.de*

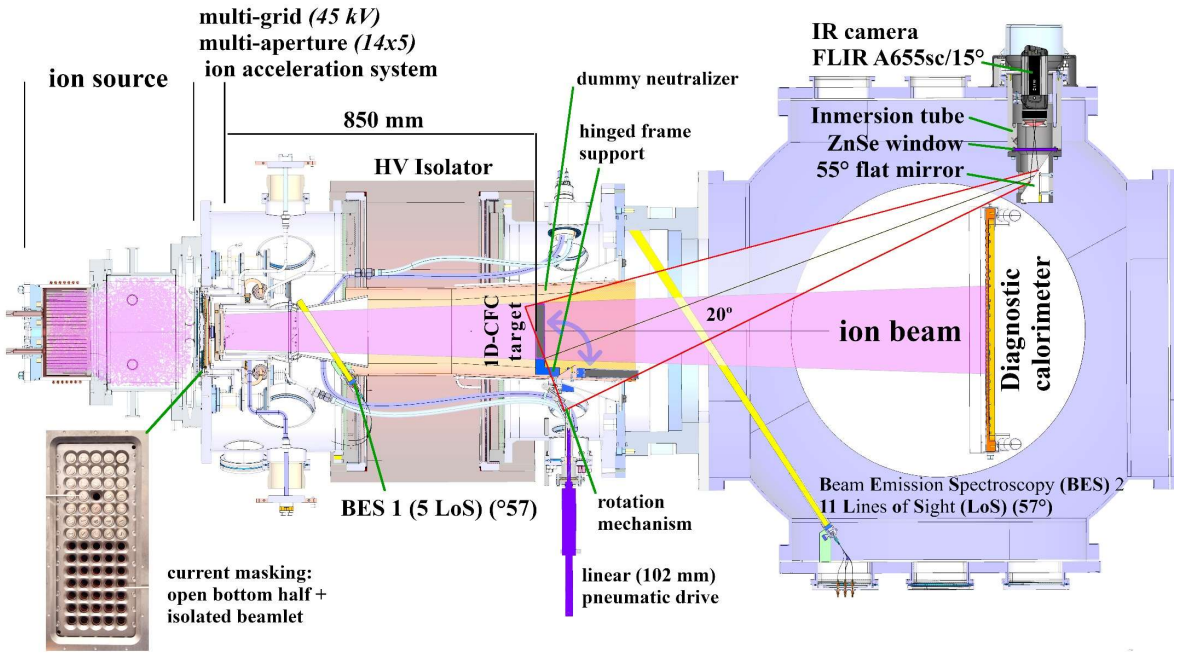


*Figure 1: Horizontal cut-out view of the BATMAN Upgrade, with its main components and beam diagnostic tools labelled.*

This paper describes the design of a new 1D-CFC beam target diagnostic tool, placed at 851 mm from the acceleration system that can be rotated in and out of the beam. It presents a strategy to operate it safely, avoiding the formation of cracks due to thermomechanical stress. In the last section, the reconstruction of a single beamlet power load distribution, based on FEM thermal analysis of the target is addressed. A possible evaluation strategy of the experimental data obtained from the IR camera and its accuracy are discussed.

## 2. The new 1D-CFC beam target diagnostic

The installed 1D-CFC beam target is manufactured by TOYO TANSO CO. LTD., under the commercial name, CX-1001U®, with dimensions 376×142×20 mm³. In this work, FEM analysis (ANSYS®) are performed with the non linear thermal material properties, provided by the manufacturer [7] and assuming linear mechanical properties at room temperature for the whole temperature range as in [8] [9].

The target is placed with its face perpendicular to the beam and centered with respect the extraction grids at a distance of 851 mm from the beam acceleration system, similar to peer testbeds[4] [10] [11]. It intercepts over 90 % of the beam power at any operational scenario. At this distance, by good beam optics conditions (beamlet divergence below 9.5 mrad) the overlapping of the beamlets should be low enough so that the single beamlets can be spatially resolved.

### 2.1. Target positioning and rotation mechanism

The target is positioned inside a thin-walled copper conduit, the "dummy neutralizer", since the neutralization feature is not used in BUG. The target fits into a frame built out of two Cu-OFE slotted supports on top and bottom, connected on one side with a Mo strip. The supports are connected to the rotation axis on the outer side of the dummy neutralizer through two openings in the thin copper wall. The axis pivots ~90° in two dry stainless steel ball bearings to rotate the target in and out of the beam path. When not used, the target is positioned parallel to the inner wall of the dummy neutralizer, at few mm distance, where it is protected from the beam by a Cu-OFE wedge, the protecting element. The axis is rotated by a crank-slider mechanism built by a length adjustable rod and two pin joints attached to a vacuum pneumatic linear drive (Kurt J. Lesker© – KLPDCBP) with a maximum travel length of 102 mm at the middle plane (see Figure 1). The speed of the actuator can be adjusted but since the target is conceived to be rotated within beam pauses, the position change is slow (~5 s), which results in lower dynamic loads, less wear of components and longer operation lifetime.

### 2.2. IR optical system with sub-mm resolution

The 1D-CFC tile is being observed with an external IR camera installed in a port on the testbed vacuum tank. The aim is to observe the whole back side of the beam target with a fully focused frame and the highest spatial resolution possible. The selected LWIR Camera is the

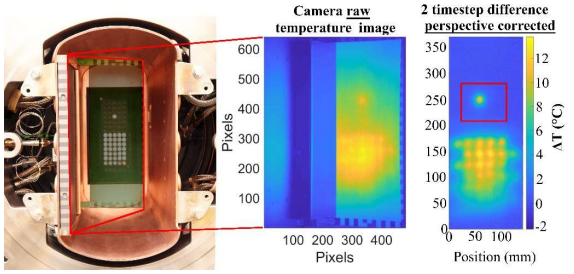


*Figure 2: Overlay of the target, in and out of the beam (left). Exemplary raw image (center) and the calculated temperature difference between two time frames (right).*

FLIR A655sc© with a resolution of 640×480 pixels for frame rates lower or equal to 50 Hz. It sits inside a vacuum immersion tube with a ZnSe window (transmissivity >90 % in the LWIR range 7.5-14 μm). A planar Cu-OFE mirror (flatness <1 μm, Ra <7 nm), inclined by 55°, grants visual access to the region of interest (sketched on Figure 1). A teleobjective (angle of view 15°) makes it possible to get the full target in frame over the 1.6 m distance, filling almost half of the image (see Figure 2 center). This results in a high resolution image, below 0.7 mm/pixel. The IR camera is mounted on a rigid support that can be rotated and finely tilted allowing picture reframing. The relative flat angle (20°) of the camera viewing cone to the target normal implies that less depth of field is required to obtain a fully focused image. The full focusing of the image is confirmed by direct observation of the alignment patterns stenciled with graphite spray onto the support frame (Figure 2 center). The post-processing of the images follows with cropping of the back of the target, perspective correction and finally, pixel-to-mm scaling (Figure 2 right). The next step concerning the analysis of the temperature profiles obtained from the rear side of the target and its correlation with the heat flux footprint on the front, is discussed on paragraph 4.

## 3. Safety analysis and interlock definitions

The dummy neutralizer is the only (inertially) cooled component in the vicinity of the target and therefore the only heat sink. The temperature of the protecting element and the two target supports is monitored by four thermocouples.

The 1D-CFC material of the target has implicit high temperature resistance. Its operational limit is defined by the maximum allowable tensile stress of 3 MPa though, above which the carbon matrix in between the carbon fibers cracks open [9]. Thermo-mechanical FEM analyses are performed for the two outmost base experimental scenarios possible with the BUG acceleration system. The first with the highest total power (HP) and second with the lowest divergence (LD), for both configurations, with and without masking. Thermal radiation is included assuming an emission coefficient of ε = 0.8 but neglecting any thermal contact, for simplicity. Mechanically the material is assumed to behave elastically. The operational parameters of BUG are summarized in Table 1. The input heat flux profiles on the front side of the target are calculated as in [12] with the beam optics code IBSimu and the IPP geometrical beam code ABC3D (on Figure 3)

Table 1. Summarizing parameters for the base experimental scenarios.

| | HP | HP masked | LD | LD masked |
|---|---|---|---|---|
| $U_{ext} + U_{acc} = U_{tot}$ (kV) | 10 + 35 | | 5 + 35 | |
| $I_{ext}$ (mA/aperture) | 46 | | 23 | |
| aperture ⌀ (mm) | 14 | | | |
| min core div (mrad) | 40.5 | | 8.5 | |
| Min beamlet σ (mm) on target | 28 | | 8.1 | |
| N° of apertures | 70 | 36 | 70 | 36 |
| $P_{beamlet}$ (W) | 2100 | | 920 | |
| $P_{tot}$ (kW) | 145.5 | 74.8 | 64.6 | 33.2 |
| $q''_{max}$ (MW/m²) | 5 | | 2.3 | |

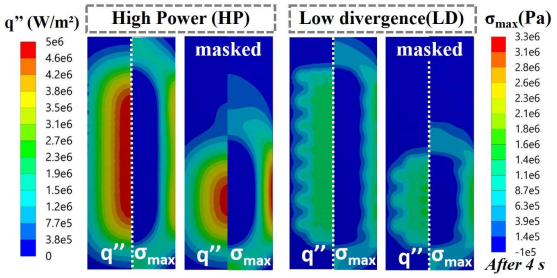


*Figure 3: Outmost heat flux (q") scenarios analyzed and their corresponding maximum principal mechanical stress ($\sigma_{max}$) fields calculated after 4 s.*

The FEM simulations show that mechanical failure starts at the colder sides of the target (see Figure 3), caused by inhomogeneous deformation due to the strongly inhomogeneous temperature (or heat flux) distribution. Extra cases have been calculated by scaling down the total power but keeping the heat flux profiles of the base scenarios. This is especially useful for the 44 % HP case, whose total power matches that of the LD scenario, so that the impact of better beam optics on the mechanical stress distribution can be inferred from it.

### 3.1. Energy interlock for intermittent operation

A time-based safety interlock has been previously proposed for such 1D-CFC beam targets [9], determined from the total beam acceleration voltage ($U_{tot}$) setting and estimating the resulting total accelerated ion current ($I_{tot}$). Besides the uncertainty when guessing $I_{tot}$, the method does not consider any effect derived from the intermittent operation of the target. The target is heated up during beam pulse but in the pauses it cools down and the temperature on the target homogenizes, reducing the mechanical stress until the next beam pulse comes.

An energy-based approach is more suitable to track the condition of the target, so it is possible to define an energy limit ($E_{lim}$) that the target can absorb before mechanical failure occurs. During beam pulse the beam power measured electrically ($U_{tot}$×$I_{tot}$) is time-integrated and added to the "energy capacity" of the target. An $E_{lim}$ can be determined for each scenario with the energy versus mechanical stress graphs obtained via FEM simulations (in Figure 4), applying the 3 MPa limit. There is a large spread among the scenarios and three main effects can be identified. The largest effect is caused by

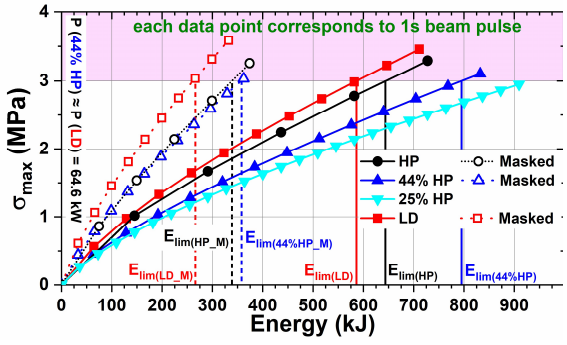


*Figure 4: Summing up result of the thermomechanical FEM calculation for the considered cases.*

the masking: heating just half of the target makes this half expand thermally, while the other half remains cold and does not expand, creating even larger mechanical stress. The $E_{lim}$ of the masked cases is a factor $\alpha_{mask}$ of ~0.4 with respect to the case without the mask, as calculated from $E_{lim(HP\_M)} / E_{lim(HP)} \approx E_{lim(LD\_M)} / E_{lim(LD)} \approx E_{lim(44\ \%HP\_M)} / E_{lim(44\ \%HP)}$ on Figure 4. Second, better beam optics reduces the $E_{lim}$ by a factor of $\alpha_{div}$ of ~0.7 compared to worse beam optics, for the same heating power, as found from $E_{lim(LD)}/E_{lim(44\ \%HP)} \approx E_{lim(LD\_M)}/E_{lim(44\ \%HP\_M)}$ (on Figure 4). Third, the higher the heating power, the lower the $E_{lim}$ is for same beam optics and masking conditions. A general $E_{lim}$, defined as interlock needs to be safe but not too constraining. Our proposal is to set $E_{lim(HP)}$ as a reference with a safety reserve $S_R$ (suggested is $S_R$=0.75) and apply the previously obtained factors ($\alpha_{mask}$ and $\alpha_{div}$), depending on the kind of experiments that are planned. Exemplarily, the $E_{lim}$ for low divergence studies with masking should be described as $E_{lim} = E_{lim(HP)} \times S_R \times \alpha_{mask} \times \alpha_{div} = 645 \times 0.75 \times 0.4 \times 0.7 = 135.4$ kJ.

During beam pauses, the temperature of the target homogenizes (decrease of $T_{max} - T_{min}$) with an exponential decay behavior (as on Figure *5*), which

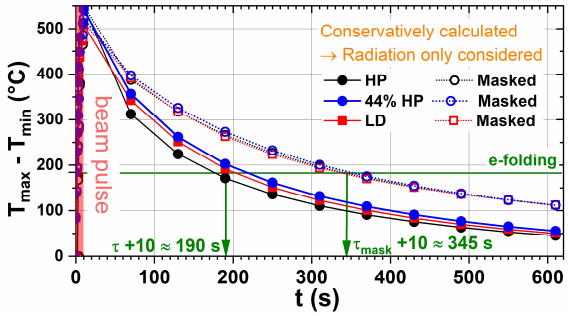


*Figure 5: Cool down curves for the target for the different scenarios, reaching a maximum temperature difference around 500°C.*

correlates with the mechanical stress. The maximum 3 MPa limit is reached, when $T_{max} - T_{min} \approx 500$°C. The homogenization of the temperature can be then interpreted as the recovery of the capacity to absorb energy. From the cooling down curves on Figure *5*, two different time constants ($\tau$ and $\tau_{mask}$) can be obtained depending on whether the acceleration system is masked or not. The energy-based interlock condition is expressed mathematically as follows:

$$\boldsymbol{E_{lim}} \cdot \left(\mathbf{1} - \boldsymbol{e}^{-\frac{\boldsymbol{t_{cooling}[s]}}{\boldsymbol{\tau}}}\right) - \int_{\boldsymbol{t_0}}^{\boldsymbol{t}} \boldsymbol{U_{tot}(t)[V] \cdot I_{tot}(t)[A] \cdot dt} > \mathbf{0}$$

## 4. Analysis of a simulated beamlet

The IR camera delivers a timestamped temperature field of the back of the target, while the goal is to assess the heat flux profiles on the front side. The temperature fields allow accurate location of the beamlets. The correlation between back temperature and the front heat flux is studied through FEM simulations, specifically for the CX-1001U® material properties and the thickness (20 mm) of the IPP target and for a single beamlet, representing the isolated beamlet in the current BUG configuration. The heat flux of the beamlet has been

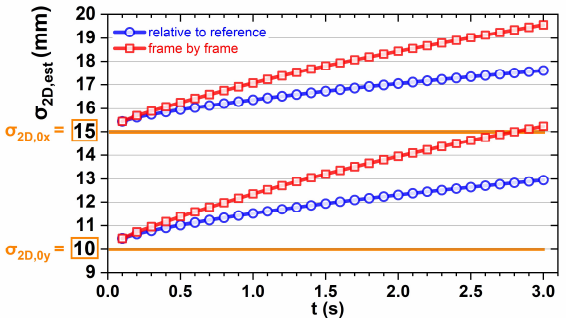


*Figure 6: 2D Gaussian fit ($\sigma_{2D,est}$) of the temperature profiles at the back of the target along the first 3 s of a simulated beam with a 2D-Gaussian heat flux distribution with shape parameters: $\sigma_{2D,0x}$ = 15 mm and $\sigma_{2D,0y}$ = 10 mm.*

modeled as a 2D-Gaussian distribution, a commonly accepted beamlet shape, for different 2D-Gaussian widths ($\sigma_{2D}$), from 5 to 25 mm, stepwise every 2.5 mm and beamlet power, from (250), 500 - 2500 W, stepwise every 500 W; covering the likely operating space at BUG.

### 4.1. Proposed temperature analysis and accuracy

For the analysis, it should be considered that, due to the subsequent beam pulse repetition on the target after the first beam pulse of the day, the target temperature is not uniform at the beginning of each beam pulse. Therefore, the analysis starts by calculating the difference between two temperature time frames. Two methods can be used, the first one is based on selecting a frame just before beam start as a reference which is then subtracted from every frame, while in the second, every frame is subtracted from its precedent, frame by frame. A comparison of both methods is shown in Figure *6* for an assumed ellipsoidal beamlet footprint with shape paremeters: $\sigma_{2D,0x}$ = 15 mm and $\sigma_{2D,0y}$ = 10 mm. The effect of lateral heat conduction, which broadens the temperature profile, can be qualitatively very well visualized. The earlier the time frame after beam pulse start is chosen for estimation of the heat flux shape, the lower the error. Regarding the temperature difference methods, both perform similarly at the very first tenths of second but using a reference frame results in lower errors at later times, so this one is selected for the error estimation graph shown on Figure 7. Within the first 0.2 s the heat flux profile shape can be quite accurately

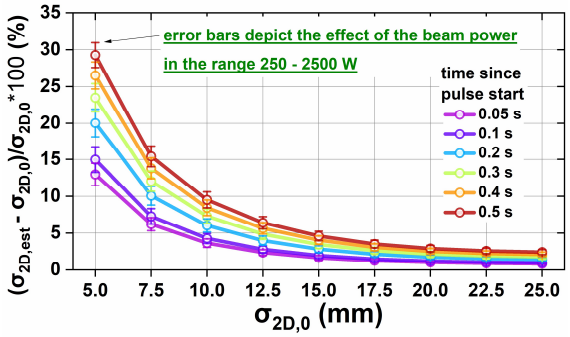


*Figure 7: Estimation error between the 2D Gaussian shaped heat flux with defined widths ($\sigma_{2D,0}$) and the estimated width ($\sigma_{2D,est}$).*

predicted with the temperature profile with a relative error below 25 % in the studied operating space. The relative error is always overestimating and inversely proportional to the width of the heat flux profile. This depends also very little on the beam transported power.

## 5. Conclusion and outlook

A new beam diagnostic tool for the negative ion source experiment BATMAN Upgrade has been designed, manufactured and commissioned. It consists of the IR imaging of the back of a 1D-CFC target which is exposed to a beam of beamlets at a close distance from the beam acceleration system. An IR imaging system displays the whole target with a pixel resolution better than 0.7×0.7 mm². A safety analysis of its operation has been done and an energy-based interlock is presented that considers its intermittent operation and the cooling down phases in between beam pulses.

An analysis on simulated 2D-Gaussian shaped, single beamlets within the operational space of BUG shows that the temperature profile shape at the back of the target should correlate relatively well with the heat flux on the front by selecting the earliest temperature frames. The relative error is below 25 % within the first 0.2 s for $\sigma_{2D} \geq 5$ mm, decreasing quickly for larger widths. The power transported by the beam has a little impact on the accuracy of the method in the studied space, assuming that at lower power, the worse signal to noise ratio of the temperature might render the analysis more difficult. This calculated errors can be used to correct down the obtained experimental data or to define the always overestimating error bars.

The next step will be to obtain, together with the position and the shape of isolated beamlet, the actual beamlet power impinging on the target and assess its estimation errors. The further step is applying the analysis to the full beam of beamlets.

## Acknowledgments

This work has been carried out within the framework of the EUROfusion Consortium and has received funding from the EURATOM research and training programme 2014-2018 and 2019-2020 under grant agreement No. 633053. The views and opinions expressed herein do not necessarily reflect those of the European Commission.

## References

[1] R. Hemsworth et al, New J. Phys. 19,025005 (2017); https://doi.org/10.1088/1367-2630/19/2/025005

[2] B. Heinemann et al, AIP Conference Proceedings 1655, 060003 (2015); https://doi.org/10.1063/1.4916472

[3] G. Serianni et al, Rev. Sci. Instrum. 85, 02A736 (2014); https://doi.org/10.1063/1.4861391

[4] A. Rizzolo et al, Fusion Eng. Des. 85, 2268-2273 (2010); https://doi.org/10.1016/j.fusengdes.2010.09.003

[5] P. Sonato et al, Fusion Eng. Des. 84, 269-274 (2009); https://doi.org/10.1016/j.fusengdes.2008.11.095

[6] C. Wimmer et al, Rev. Sci. Instrum. 91, 013509 (2020); https://doi.org/10.1063/1.5129336

[7] Material CX-1001 Technical Data Sheet T05-022-003 Rev.1 - from manufacturer TOYO TANSO CO., LTD

[8] M. Dalla Palma et al, J Therm Anal Calorim 134, 143-155 (2018); https://doi.org/10.1007/s10973-018-7430-5

[9] A. Pimazzoni et al,.Fusion Eng. Des. 146 B, 2457-2461 (2019); https://doi.org/10.1016/j.fusengdes.2019.04.018

[10] V. Antoni et al, AIP Conf. Proc 1655 (2015) 060005; https://doi.org/10.1063/1.4916474

[11] M. Ichikawa et al, AIP Conf. Proc 1869 (2017) 030024; https://doi.org/10.1063/1.4995744

[12] N. den Harder, Fusion Eng. Des. 153, 111507 (2020); https://doi.org/10.1016/j.fusengdes.2020.111507